

Influence of Growth Rate on Microstructural Length Scales in Directionally Solidified NiAl-Mo Hypo-Eutectic Alloy

JIANFEI ZHANG,^{1,3} XUEWEI MA,¹ HUIPING REN,¹ LIN CHEN,¹
ZILI JIN,¹ ZHENLIANG LI,¹ and JUN SHEN²

1.—College of Materials and Metallurgy, Inner Mongolia University of Science and Technology, Bao'tou 014010, People's Republic of China. 2.—State Key Laboratory of Solidification Processing, Northwestern Polytechnical University, Xi'an 710072, People's Republic of China. 3.—e-mail: zhangjianfei_vip@163.com

In this article, the Ni-46.1Al-7.8Mo (at.%) alloy was directionally solidified at different growth rates ranging from 15 $\mu\text{m/s}$ to 1000 $\mu\text{m/s}$ under a constant temperature gradient (334 K/cm). The dependence of microstructural length scales on the growth rate was investigated. The results show that, with the growth rate increasing, the primary dendritic arm spacings (PDAS) and secondary dendritic arm spacings (SDAS) decreased. There exists a large distribution range in PDAS under directional solidification conditions at a constant temperature gradient. The average PDAS and SDAS as a function of growth rate can be given as $\lambda_1 = 848.8967 V^{-0.4509}$ and $\lambda_2 = 64.2196 V^{-0.4140}$, respectively. In addition, a comparison of our results with the current theoretical models and previous experimental results has also been made.

INTRODUCTION

Dendrite structures are frequently observed during the solidification of alloys. The dendritic structure is a key microstructural feature that is generally characterized by the primary (PDAS, λ_1) and secondary (SDAS, λ_2) dendritic arm spacings. In particular, the λ_1/λ_2 ratio can be used to estimate the permeability of the mushy zone.¹ The spacing among primary and secondary is important since it determines the spacing of precipitates or porosity and, thus, has a considerable effect on the mechanical properties of solidified alloys. Because of this correlation, a significant amount of work in both theoretical and experimental research on the selection mechanism of the cellular/dendritic spacing is reported in the literature that characterizes the variation of PDAS and SDAS with alloy composition (C_0), growth rate (V), and temperature gradient (G_L) in the melt.^{2–14} Hunt and Kurz and Fisher have proposed the theoretical models to characterize cell/primary dendrite spacings as a function of growth rate, temperature gradient, and alloy composition.^{9,10} The Trivedi model is a result of the modification of the Hunt model, and it is used as a marginal stability criterion.¹¹ Hunt and Lu have proposed an analytical expression for

corresponding cellular spacing from their numerical predictions of the lower limit of stable cellular/dendritic spacing.¹² For clarity, Table I lists the theoretical models for λ_1 and λ_2 , respectively, all of which indicated that increasing the growth rate will decrease the value of λ_1 and λ_2 . In addition, current studies have claimed the existence of an allowable range of stable spacings. This has been interpreted in such a way that no unique spacing selection is stable under given experimental conditions, while the average spacing of dendritic arrays is remarkably history dependent on solidification parameters (V , G_L). Up to now, many experimental studies in the literature have compared with these theoretical predictions under steady-state growth conditions. For alloys of different systems: Pb-Sn,¹⁵ Cu-Mn,¹⁶ Pb-Bi,¹⁷ succinonitrile-carbon tetrabromide,¹⁸ Al-Zn,¹⁹ Al-Cu,²⁰ and Pb-Sb,²¹ the agreement between theory and experiment is generally reported. However, only limited information is available in the literature about the dendritic structure in intermetallic compounds.²² If nonequilibrium conditions prevail during solidification of intermetallic compounds, these materials become very important for structural applications.²³ In recent years, intermetallic NiAl alloy has been the focus of considerable research because it is expected to be a potential

Table I. Models for primary and secondary dendritic arm spacing

Models	Equations
Hunt model ⁹	$\lambda_1 = 2.83[m_L(k_0 - 1)D_L\Gamma]^{0.25}C_0^{0.25}V^{-0.25}G_L^{-0.5}$ (1)
Kurz-Fisher model ¹⁰	$\lambda_1 = 4.3\left[\frac{m_L(k_0-1)D_L\Gamma}{k_0^2}\right]^{0.25}C_0^{0.25}V^{-0.25}G_L^{-0.5}$ (2)
Trivedi model ¹¹	$\lambda_1 = 2.83[m_L(k_0 - 1)D_L\Gamma]^{0.25}C_0^{0.25}V^{-0.25}G_L^{-0.5}$ (3)
Hunt-Lu model ¹²	$\lambda_1 = 8.18k_0^{-0.335}(k_0\Delta T_0)^{-0.41}\Gamma^{0.41}D_L^{0.59}V^{0.59}$ (4)
Trivedi and Somboonsuk model ¹³	$\lambda_2 = \left(\frac{8\Gamma D_L L}{k_0 V \Delta T_0}\right)^{0.5}$ (5)
Bouchard-Kirkaldy model ¹⁴	$\lambda_2 = 2\pi a_2 \left(\frac{4\Gamma}{C_0(1-k_0)^2\Delta H} \left(\frac{D_L}{V}\right)^2\right)^{1/3}$ (6)

m_L , liquidus slope; k_0 , equilibrium distribution coefficient; D_L , diffusion coefficient in the liquid; Γ , Gibbs-Thomson coefficient; G_L , temperature gradient; V , growth rate; C_0 , initial alloy composition; a_2 , secondary dendrite calibrating factor. According to Bouchard' analysis, for NiAl, $a_2 = 4$ (Ref. 14); L , a constant that depends on harmonic perturbations. According to Trivedi's analysis, for dendritic growth, the value of L is equal to 28; ΔH , heat of fusion; ΔT_0 , equilibrium solidification temperature range $\Delta T_0 = \frac{m_L(k_0-1)C_0}{k_0}$

candidate material in the automotive and aerospace industries for high-temperature structural applications.²⁴ In the present work, NiAl-7.8Mo hypo-eutectic alloy was chosen for investigating the effect of the growth rate on the microstructural characteristic length scales of the primary NiAl phase (PDAS and SDAS) and for comparing the results with the existing theoretical models.

EXPERIMENTAL PROCEDURE

Alloy Preparation and Directional Solidification

In the present work, the master alloy with a composition of Ni-46.1Al-7.8Mo (at.%, which will be the same throughout this article unless otherwise stated and referred to as NiAl-7.8Mo for short) was prepared by induction melting under Ar atmosphere and dropped into a cylindrical ingot measuring 80 mm in diameter and 100 mm in length. The purity of raw materials used in this study is Ni 99.99% (wt.%), Al 99.99% (wt.%), and Mo 99.95% (wt.%), respectively. Directionally solidified (DS) rods were cut from the master ingot into $\Phi 3.9 \times 100$ -mm cylinder bars by a wire electrodischarged machine (EDM) and placed into a high-purity alumina crucible of 4/5 mm diameter (inside/outside diameter). Directional solidification experiments were performed under an argon atmosphere in a Bridgman-type crystal growing facility with liquid metal cooling (LMC) technique. The alumina crucible with the as-cast rod was positioned in the furnace and heated up to $\sim 1700^\circ \pm 10^\circ$ with a graphite heater by induction heating and then kept for 30 min for melt homogenization. The upper part with the heating element was then slowly and uniformly shifted downward to allow unidirectional heat extraction. This operation was controlled by a servomotor at various withdraw rates. After the solidified distance reached 50 mm, the sample was quenched into liquid Ga-In-Sn alloy to obtain the

interface growth morphology and to study the formation of the microstructure. A thermal gradient at the S/L interface is approximately 334 K/cm, and the details of the measuring temperature gradient are given in Ref. 25. The samples were grown at different rates varying from 15 $\mu\text{m/s}$ to 1000 $\mu\text{m/s}$. The experiment was carried in the same furnace and in the same experimental condition. Here we assume that the thermal conditions stay identical and focus on discussing the influence of growth rate on microstructural length scales.

Metallography and Measurement of Microstructural Length Scales

After solidification, the directionally solidified samples were sectioned transversely and longitudinally by EDM for metallographic analysis. The metallographic process involved grinding, mechanical polishing, and chemical etching with a solution of 80% HCl-20% HNO₃. We revealed and analyzed the etched specimens by using a scanning electron microscopy (SEM) equipped with energy-dispersive spectrometry (EDS). The quantitative image analysis was conducted by means of SISCAS V8.0 metallographic image analysis software. The PDAS was obtained by measuring the distance between the nearest two dendrite tips on the transverse section, and the SDAS was measured by averaging the distance between adjacent side branches on the longitudinal section of a primary arm. About 90–120 values of λ_1 , λ_2 for each growth rate were measured to increase statistical sensitivity.

RESULT AND DISCUSSION

Microstructure of Directionally Solidified NiAl-7.8Mo Alloy

The typical quenched S/L interfaces and transverse section microstructures of the DS NiAl-7.8Mo alloy with increasing growth rate in the range of

15 $\mu\text{m/s}$ to 1000 $\mu\text{m/s}$ at $G_L=334$ K/cm are shown in Fig. 1. The solidification structure presents a mixed structure, that is, dendrites of the β NiAl phase and interdendritic two-phase eutectic ($\alpha\text{Mo}+\beta\text{NiAl}$). The solid-liquid interface presents the competitive growth of the NiAl phase and the eutectic ($\alpha\text{Mo} + \beta\text{NiAl}$). A fast growth rate produces fine and highly oriented dendrites, while a slow growth rate produces large and coarse dendrites. For the hypoeutectic composition selected for the present investigation, due to the long-range boundary layer built up ahead of the solid-liquid interface, the NiAl

phase becomes heavily constitutionally undercooled and tends to grow faster than the eutectic. It can be found that the NiAl dendrites form prior to growth of the eutectic. The eutectic then completes solidification by filling in the areas surrounding the dendrites. The αMo phases present a fibrous morphology. The resulting structures contain the primary βNiAl phase (black dendrites) and the eutectic ($\alpha\text{Mo} + \beta\text{NiAl}$).

The quantitative chemical composition analysis of the eutectic and the primary NiAl phase was carried out by using EDS and is given in Fig. 2. Here we

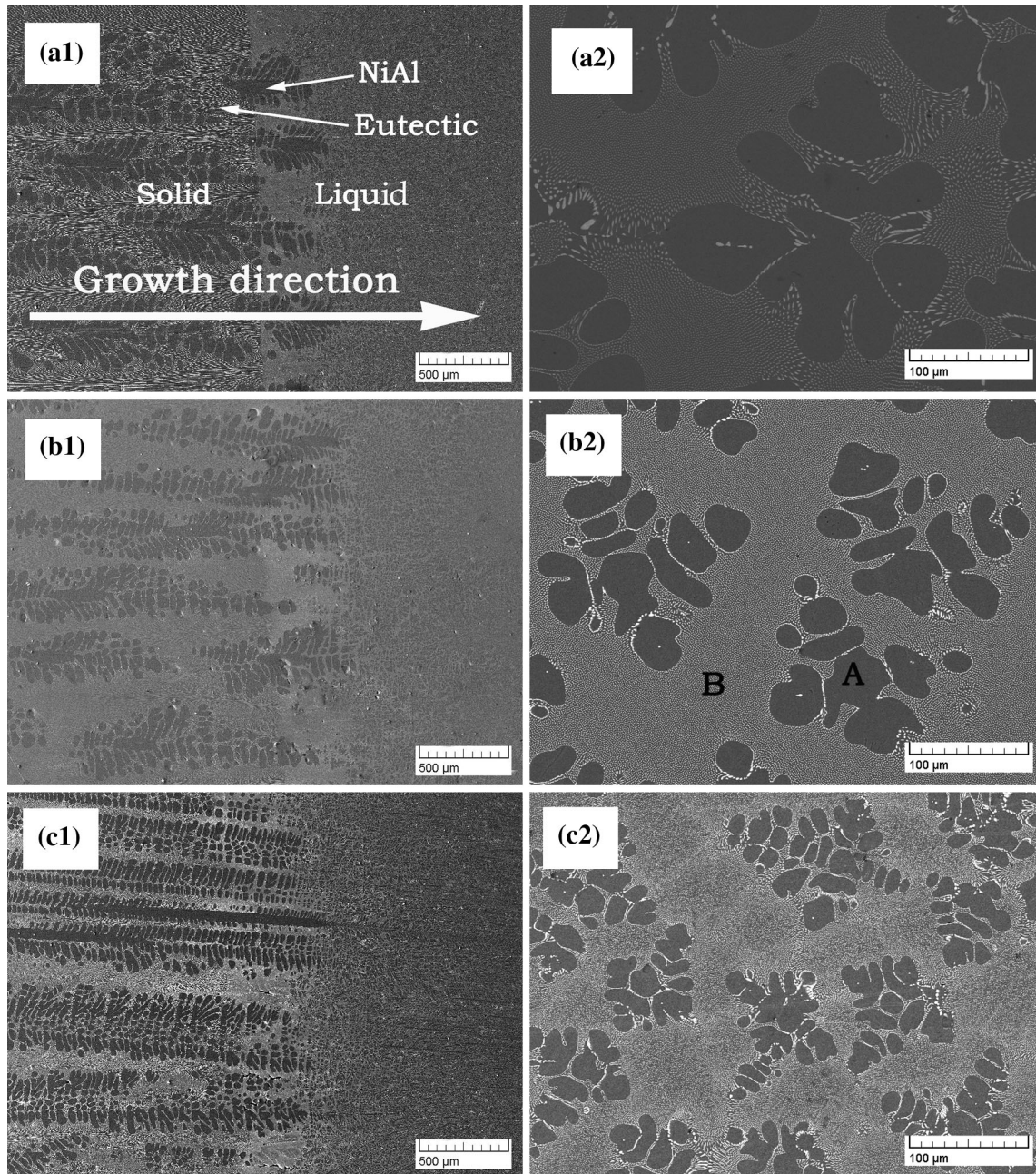


Fig. 1. SEM micrographs of DS microstructures under different growth rates for the NiAl-7.8Mo alloy: (a) 15 $\mu\text{m/s}$; (b) 25 $\mu\text{m/s}$; (c) 50 $\mu\text{m/s}$; (d) 100 $\mu\text{m/s}$; (e) 300 $\mu\text{m/s}$; and (f) 1000 $\mu\text{m/s}$. The subscripts 1 and 2 denote longitudinal and transverse microstructures, respectively.

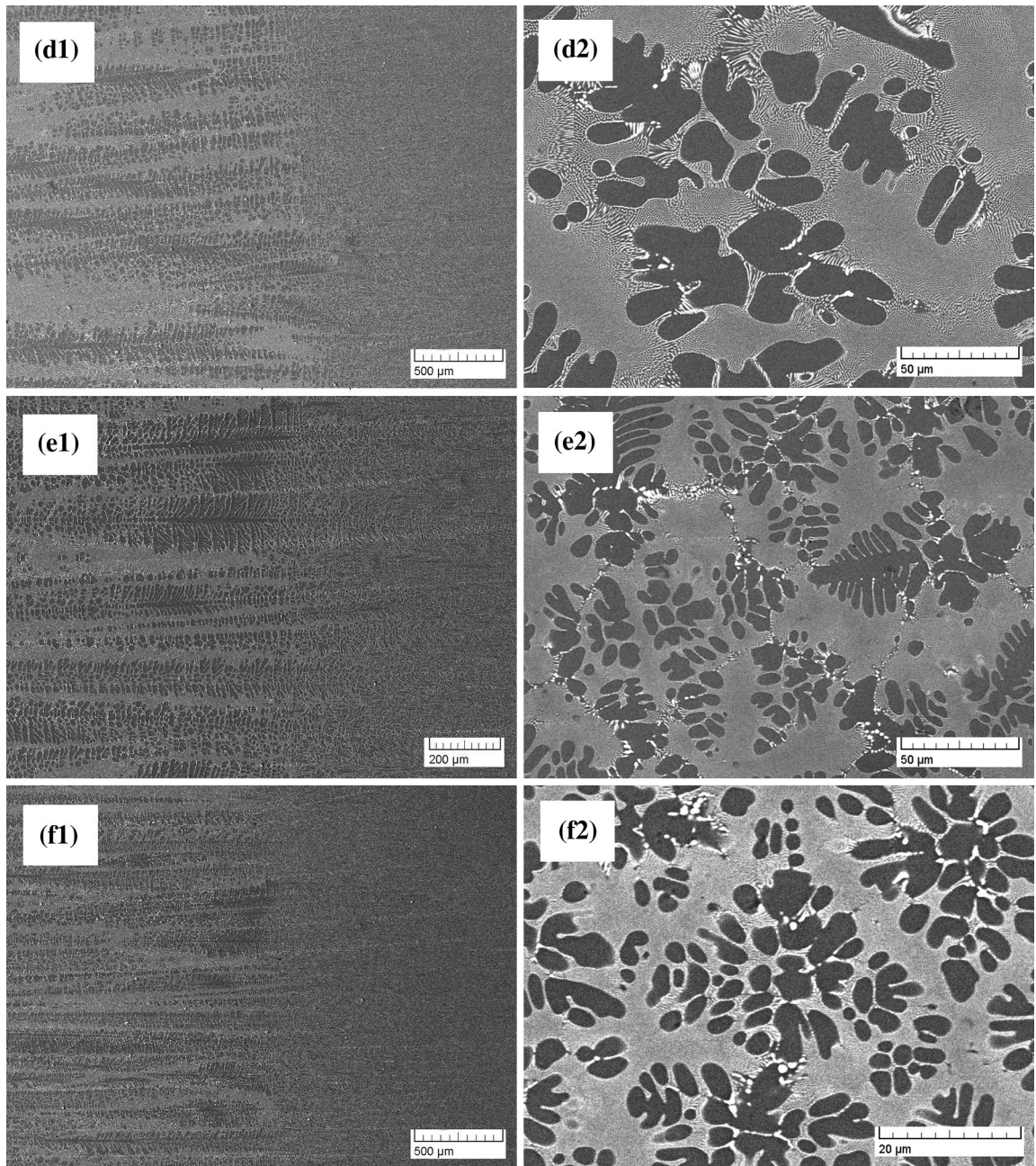


Fig. 1. continued.

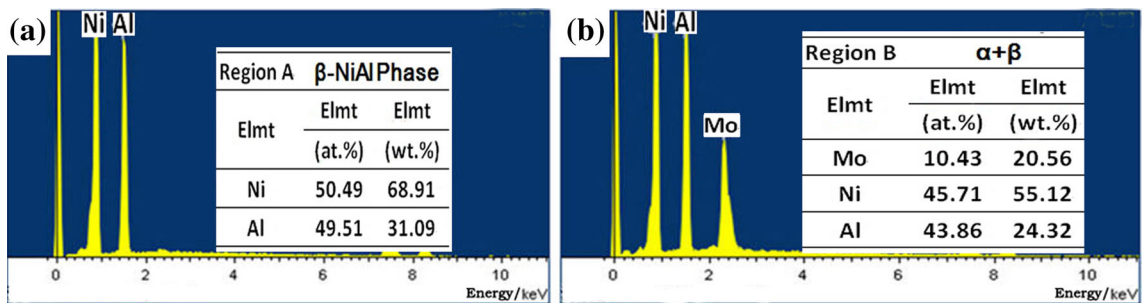


Fig. 2. Chemical composition analysis of DS microstructures of NiAl-7.8Mo alloy by SEM-EDX ($V = 25 \mu\text{m/s}$, $G = 334 \text{ K/cm}$): (a) dark primary NiAl phase; (b) bright gray eutectics

selected the sample of $V = 25 \mu\text{m/s}$ to determine the compositions of the constituent phases. It was found that the NiAl phase contained no Mo and had the near-stoichiometric composition Ni50.49-Al49.51, whereas the eutectic contained all three elements and had the composition Ni45.71-Al43.86-Mo10.43.

Effect of Growth Rate on the Dendritic Spacing

Table II gives the measurement results of dendritic spacing obtained at $G_L = 334 \text{ K/cm}$, where $\lambda_{1\text{max}}$, $\lambda_{1\text{min}}$, and $\lambda_{1\text{mean}}$ are maximum, minimum, and average primary spacing, respectively. It is shown that there exists a large distribution range in primary spacing with the variation of growth rate from $15 \mu\text{m/s}$ to $1000 \mu\text{m/s}$. As the growth rate increases, the distribution range tends to slightly decrease. The ratio of maximum spacing to the minimum value, as a function of growth rate, varies between 2.6272 and 3.6177. A clear distribution range of primary spacings, as a function of growth rate, is shown in Fig. 3, which is plotted from the data in Table II. Through regression analysis, we obtain $\lambda_{1\text{max}} = 1230.4234 V^{-0.4399}$, $\lambda_{1\text{min}} = 382.5920 V^{-0.4344}$, and $\lambda_{1\text{mean}} = 848.8967 V^{-0.4509}$. Gao et al.²⁶ and Min et al.²⁷ reported their experimental results on the primary dendritic spacings of superalloy DD3 and

DZ125 under a directional solidification condition. It was found that, for DD3 and DZ125 alloys, the average primary spacing and the growth rate obey $\lambda_1 V^{0.24} = \text{const.}$ with a smaller exponent than ours. However, the exponent value of the growth rate 0.4509 in our result is very close to the values 0.50, 0.50, and 0.44, which were obtained by Kloosterman et al.²⁸ for Al-Ni alloy, Ma et al.²⁹ for Zn-Cu alloy, and Klaren et al.³⁰ for Pb-Au alloy, respectively. The discrepancies may be caused by the experimental condition and the alloy system. The values of the exponent on the scaling of the primary spacing λ_1 with the velocity for different alloy systems are summarized by Maraşlı and Çadırılı.^{2,3} By a comparison of the results we can find out that the exponent values are different in the different alloy systems and that the exponent values have a certain differences even in the same alloy system. So, it is probable that the exponent value might depend on the alloy systems and experimental conditions.

To compare our experimental results with theoretical model, the predictions of four theoretical models (as described by Eqs. 1–4 in Table I) were considered. By using the physical parameters given in Table III, the predictions of four theoretical models (as described by Eqs. 1–4 in Table I) were compared with the measured primary spacing, as

Table II. Measured experimental data (PDAS and SDAS) of DS NiAl-7.8Mo alloy

Growth rate V ($\mu\text{m/s}$)	PDAS λ_1 (μm)				SDAS λ_2 (μm)	λ_1/λ_2
	$\lambda_{1\text{max}}$ (μm)	$\lambda_{1\text{min}}$ (μm)	λ_1 (μm)	$\lambda_{1\text{max}}/\lambda_{1\text{min}}$		
15	381.0	115.3	246.809	3.3044	20.445	12.0719
25	257.9	95.7	195.059	2.6949	17.529	11.1278
50	264.7	66.7	156.755	3.9685	13.767	11.3863
100	179.7	68.4	115.733	2.6272	10.264	11.2756
300	81.4	22.5	57.019	3.6177	4.240	13.4479
1000	37.3	12.9	25.495	2.8915	3.258	7.8254

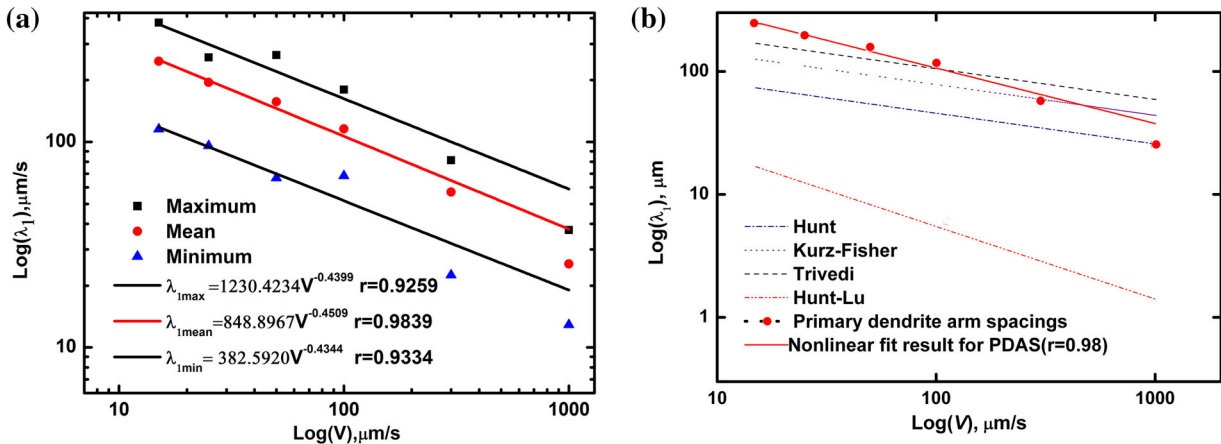


Fig. 3. Selection of SDAS as a function of growth rate: (a) comparison of PDAS of the directionally solidified NiAl-7.8Mo alloy with the predictions of the theoretical models (b).

Table III. Physical parameters of NiAl-Mo alloy

Parameter	Symbol	Units	Value
Liquidus slope of β	m_β	$\text{K}(\text{at.}\%)^{-1}$	-23.44^{31}
Gibbs–Thomson coefficient of βNiAl	Γ_β	$\text{K}/\mu\text{m}$	0.035^{32}
Diffusion coefficient	D_β	$\mu\text{m}^2/\text{s}$	6000^{33}
Partition coefficient	K_β	–	0.79^{33}
Temperature gradient	G_L	K/cm	334
Heat of fusion	ΔH	J/cm^3	16^{33}

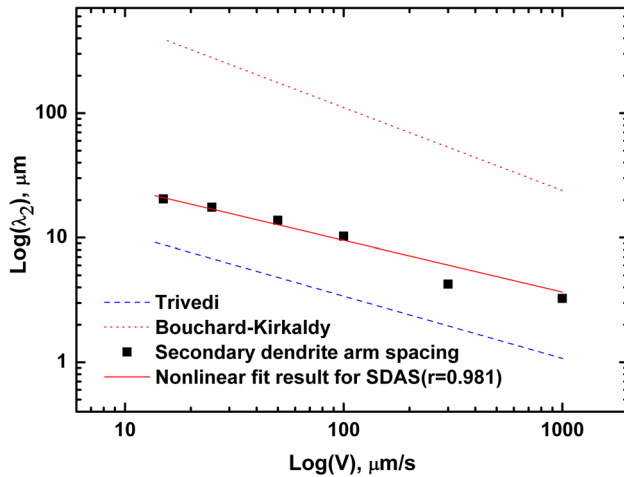


Fig. 4. Comparison of SDAS of the directionally solidified NiAl-7.8Mo alloy with the predictions of the theoretical models.

shown in Fig. 3. It is found that the prediction of the Hunt–Lu model exhibits a large deviation with the present experimental results. The calculated values for the Hunt–Lu model are a little smaller than the experimental data. The predictions of the Trivedi model and Kurz–Fisher model show reasonable parametric agreement.

Table II gives the SDAS of NiAl-7.8Mo alloy at different growth rates. It can be observed that with the increasing of the growth rate, the secondary arm spacing decreases as well. The variation of λ_2 on the $\log \lambda_2$ versus $\log V$ plot is essentially linear for the growth rate ranges (15–1000 $\mu\text{m}/\text{s}$). A linear regression analysis gives the proportionality equation as $\lambda_2 = 64.22 V^{-0.4140}$ (Fig. 4), and the exponent value 0.4140 is in agreement with Çadirli’s value 0.43 for PVA,³⁴ Kaya’s value 0.46 for SCN-CTB,⁸ and Seetharaman’s value 0.44 for $\text{CBr}_4\text{-C}_2\text{Cl}_6$.³⁵ The variation in the values of λ_2 experimentally obtained with a constant G_L at different V in the present work has been compared with the values of λ_2 calculated from the Trivedi model and the Bouchard–Kirkaldy model, which are given in Fig. 4. As shown in Fig. 4, the calculated line of λ_2 with the Trivedi model as a function of V is lower than our experimental values and the calculated line of λ_2 with the Bouchard–Kirkaldy model as function of V

exhibits a fairly larger deviation from our experimental results. This phenomenon can be attributed to the retard of coarsening of the secondary dendrite arms by solidification reaction and transformation.¹⁴ During the process of solidification, according to the solidification theory, a ripening process causes the highly branched arms to change with time into coarser, less branched, and more widely spaced ones. The driving force for the ripening process is the difference in chemical potential of crystals with varying interfacial energies due to different curvatures. Since the secondary dendrite arms continuously adjust during solidification until the end of solidification, maybe the ripening process is not sufficient or retarded. Moreover, because of the complexity of solute distribution and microstructure formation, it is difficult to make precise predictions of SDAS in a multicomponent alloy system.

The λ_1/λ_2 has been used to estimate the permeability of the mushy zone, but only limited information is available in the literature about this ratio. Cicutti and Boeri³⁶ developed an analytical model to estimate the $\lambda_1/\lambda_2 \approx 2.6$. This is consistent with the values ranging from 2 to 4 suggested by Wolf.³⁷ But it can be observed from our experimental results in Table II that the λ_1/λ_2 is not constant but ranges from 7.8254 to 13.4479 with the increase of growth rate. It is clear that our results are much bigger than that of Cicutti and Wolf.

CONCLUSION

The directional solidification experiments have been carried out on the NiAl-7.8Mo alloy. The effect of growth rate on the primary arm spacing, secondary arm spacing, and their relations between characteristic length scales are investigated. The following conclusions were obtained:

- 1) For a given C_0 of NiAl-7.8Mo hypo-eutectic alloy, over the growth rate range of 15–1000 $\mu\text{m}/\text{s}$ at $G_L = 334 \text{ K}/\text{cm}$, there exists a large distribution range in primary NiAl dendritic spacing under directional solidification conditions. With the increase of growth rate, both the average spacing and the distribution range tend to decrease. The average, maximum, and minimum primary spacing of NiAl-7.8Mo, as a function of growth rate, can be

given as $\lambda_{1\max} = 1230.4234 V^{-0.4399}$, $\lambda_{1\min} = 382.5920 V^{-0.4344}$, and $\lambda_{1\text{mean}} = 848.8967 V^{-0.4509}$, respectively. Our experimental results agree well with the Trivedi model and the Kurz–Fisher model.

- 2) With the increase of growth rate, the SDAS is decreasing too. The SDAS of NiAl-7.8Mo, as a function of growth rate, is given as $\lambda_2 = 64.2196 V^{-0.4140}$. The Trivedi model and the Bouchard–Kirkaldy model predicting the SDAS exhibit a large deviation from the experimental results during directional solidification. Our measurements fall in between the predictions of the two models tested here.
- 3) The values λ_1/λ_2 are not constant but range from 7.8254 to 13.4479 with the increase of growth rate. Its minimum value is at the growth rate of 1000 $\mu\text{m/s}$. Our results are much bigger than that of Cicutti³⁶ and Wolf.³⁷

ACKNOWLEDGEMENTS

The authors acknowledge the National Natural Science Foundation of China (No. 51564041), the Natural Science Foundation of Inner Mongolia of China (No. 2014MS0518), the Inner Mongolia University of Science and Technology Industry-Study-Research Found (No. PY201509), and the Inner Mongolia University of Science and Technology Innovation Fund (No. 2012NCL004) for financial support.

REFERENCES

1. D. Poirier, *Metall. Trans. B* 18, 245 (1987).
2. N. Maraşlı, K. Keşlioğlu, B. Arslan, H. Kaya, and E. Çadırılı, *J. Mater. Process. Technol.* 202, 145 (2008).
3. E. Çadırılı, I. Karaca, H. Kaya, and N. Maraşlı, *J. Cryst. Growth* 255, 190 (2003).
4. G.L. Ding, W.D. Huang, X. Huang, X. Lin, and Y.H. Zhou, *Acta Mater.* 44, 3705 (1996).
5. J.A. Warren and J.S. Langer, *Phys. Rev. E* 47, 2702 (1993).
6. Y.Z. Zhou and A. Volek, *Scr. Mater.* 56, 537 (2007).
7. D. Ma, W. Xu, S.C. Ng, and Y. Li, *Mater. Sci. Eng., A* 390, 52 (2005).
8. H. Kaya, E. Çadırılı, K. Keşlioğlu, and N. Maraşlı, *J. Cryst. Growth* 276, 583 (2005).
9. J.D. Hunt, *Solidification and casting of metals* (London: The Metals Society, 1979), pp. 3–9.
10. W. Kurz and J.D. Fisher, *Acta Metall.* 29, 11 (1981).
11. R. Trivedi, *Metall. Mater. Trans. A* 15, 977 (1984).
12. J.D. Hunt and S.Z. Lu, *Metall. Mater. Trans. A* 27, 611 (1996).
13. R. Trivedi and K. Somboonsuk, *Mater. Sci. Eng., A* 65, 65 (1984).
14. D. Bouchard and J.S. Kirkaldy, *Metall. Mater. Trans. B* 28, 651 (1997).
15. M. Li, T. Mori, and H. Iwasaki, *Mater. Sci. Eng., A* 265, 217 (1999).
16. Q.Y. Pan, W.D. Huang, X. Lin, and Y.H. Zhou, *J. Cryst. Growth* 181, 109 (1997).
17. X.W. Hu, S.M. Li, W.J. Chen, S.F. Gao, L. Liu, and H.Z. Fu, *J. Alloys Compd.* 484, 631 (2009).
18. N. Maraşlı, K. Keşlioğlu, B. Arslan, H. Kaya, and E. Çadırılı, *J. Mater. Process. Technol.* 202, 145 (2008).
19. J. Feng, W.D. Huang, X. Lin, Q.Y. Pan, T. Li, and Y.H. Zhou, *J. Cryst. Growth* 197, 393 (1999).
20. G.Y. An and L.X. Liu, *J. Cryst. Growth* 80, 383 (1987).
21. J. Hui, R. Tiwari, X. Wu, S.N. Tewari, and R. Trivedi, *Metall. Mater. Trans. A* 33, 3499 (2002).
22. M. Barth, B. Wei, and D.M. Herlach, *Mater. Sci. Eng., A* 226–228, 770 (1997).
23. S.V. Raj, I.E. Locci, J.A. Salem, and R.J. Pawlik, *Metall. Mater. Trans. A* 33, 597 (2002).
24. P.L. Ferrandini, F.L.G.U. Araujo, W.W. Batista, and R. Caram, *J. Cryst. Growth* 275, 147 (2005).
25. J.F. Zhang, J. Shen, Z. Shang, L. Wang, and H.Z. Fu, *Mater. Charact.* 99, 160 (2015).
26. S.F. Gao, L. Liu, Y.K. Xu, C.B. Yang, J. Zhang, and H.Z. Fu, *China Foundry* 9, 160 (2012).
27. Z.X. Min, J. Shen, Y.L. Xiong, W. Wang, Y.J. Du, L. Liu, and H.Z. Fu, *Acta Metall. Sin.* 47, 397 (2011).
28. A.B. Kloosterman and J.T.H.M. Hosson, *J. Mater. Sci.* 32, 6201 (1997).
29. D. Ma, Y. Li, S.C. Ng, and H. Jones, *Acta Metall.* 48, 419 (2000).
30. C.M. Klaren, J.D. Verhoeven, and R. Trivedi, *Metall. Trans. A* 11, 1853 (1980).
31. H.Z. Fu, L. Liu, J.J. Guo, and J.S. Li, *Directional solidification and processing of advanced materials* (Beijing: Beijing Science Press, 2008), p. 687.
32. N. Marasli and J.D. Hunt, *Acta Mater.* 44, 1085 (1996).
33. J.Q. Li and Y.L. Tang, *J. Alloys Compd.* 329, 157 (2001).
34. E. Çadırılı, N. Marasli, B. Bayender, and M. Gündüz, *Mater. Res. Bull.* 35, 985 (2000).
35. V. Seetharaman, L.M. Fabbietti, and R. Trivedi, *Metall. Trans. A* 20, 2567 (1989).
36. C. Cicutti and R. Boeri, *Scr. Mater.* 45, 1455 (2001).
37. M. Wolf (Paper presented to the Continuous Casting, Iron and Steel Society of AIME, Warrendale, 1997, pp. 259–269).